Int. J. Solids Structures, 1970, Vol. 6, pp. 37 to 52. Pergamon Press. Printed in Great Britain

ON THE BUCKLING BEHAVIOUR OF SHALLOW SPHERICAL CAPS UNDER A UNIFORM PRESSURE LOAD

S. C. TILLMAN

Civil Engineering Department, University College, Gower Street, London

Abstract—Results are presented of a theoretical and experimental investigation into the elastic buckling of clamped shallow spherical caps under a uniform pressure. Attention has been focussed on low values of the geometric parameter λ for which the symmetrical and first two asymmetrical deformation modes are valid. In the symmetrical case the results from nominally perfect shells and shells with known size of imperfection show excellent agreement with existing theory. In the asymmetrical case the theoretical work has predicted the instability of both modes after the bifurcation point and also the non-existence of a transition path between them. The experimental results however indicate a critical dependence between the final buckling loads of shells of similar λ and the rise to base radius ratio. Initial asymmetrical imperfections also seem to be important.

INTRODUCTION

IN THIS paper the asymmetrical post-bifurcation behaviour of a clamped shallow spherical cap under a uniform pressure load is investigated both theoretically and experimentally. The investigation was initiated in an attempt to explain the scatter of existing experimental buckling loads about those predicted by shallow shell theory.

The geometry of a shallow cap can be represented as in Fig. 1. Here the rise height, base radius, radius of curvature of the mid-surface and thickness of the shell are denoted by H, a, R and t respectively. The horizontal meridional, horizontal tangential and vertical displacements of a point on the shell with polar coordinates (r, θ) are denoted by U, V and W respectively. It is found from shallow shell theory (e.g. [3]) that the geometry of the shallow cap can be represented by a single parameter λ where

$$\lambda = 2[3(1-\nu^2)]^{\frac{1}{4}}\left(\frac{H}{t}\right)^{\frac{1}{2}}$$

and ν is Poisson's ratio.

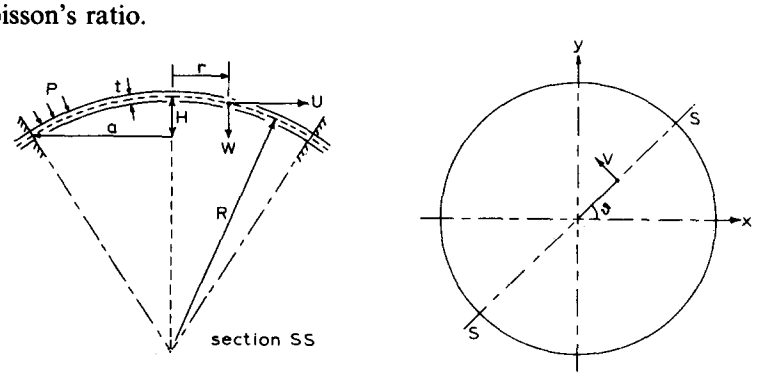

FIG. 1. Geometry of clamped shallow spherical cap.

The load-deformation relationship of the clamped cap quickly becomes non-linear after the initial application of the applied pressure and for sufficiently low values of this pressure the deformations are always axisymmetric. Furthermore, if it is assumed that the deformations always remain axisymmetric, it is found that the load reaches a limiting value P_S (point A in Fig. 2) where the shell becomes unstable and "snaps" at constant pressure to point B on the loading path. The critical pressure P_S has been theoretically investigated by Budiansky [3] for a wide range of λ and his result is shown in Fig. 3. Here P is the actual snapping pressure and P_0 the buckling pressure of the complete sphere of which the clamped cap forms part. P_0 is given by

$$P_0 = 2E\left(\frac{t}{R}\right)^2 (3[1-\nu^2])^{-\frac{1}{2}}$$

where E is Young's modulus.

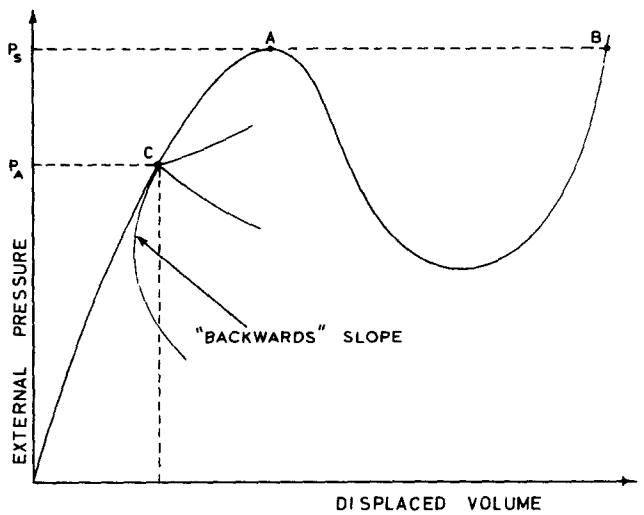

FIG. 2. Schematic equilibrium paths for a shallow clamped cap.

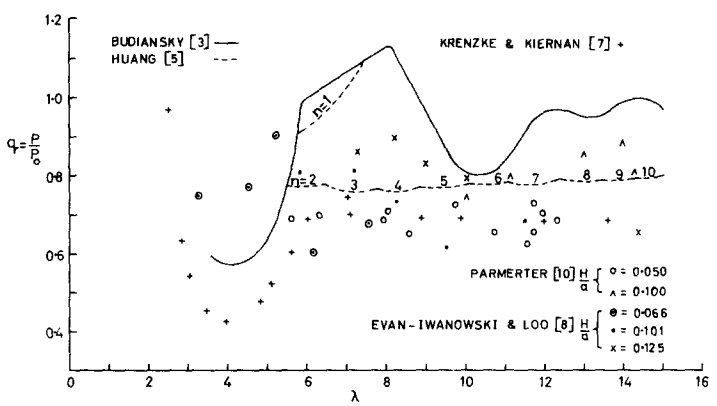

FIG. 3. Recent theoretical and experimental results.

A similar result to Budiansky has been obtained by Weinitschke [14], Thurston [12] and Archer [1].

It was shown theoretically by Huang [5] that if asymmetrical deformations were considered it was possible for shells of $\lambda \gtrsim 5{\cdot}5$ to buckle at pressures lower than P_S; that is the shell initially deforms symmetrically until it reaches point C (Fig. 2) at a pressure P_A where it bifurcates into an asymmetrical deformation mode. Huang's results for the bifurcation pressures P_A for a wide range of λ are shown in Fig. 3. Here the labels $n = 1$, $n = 2$, etc., on Huang's curves represent one, two, etc., waves in the circumferential direction of the shell. Huang's approach to the problem was to solve Marguerre's [9] non-linear shell equations by finite differences. The stability of the subsequent post-bifurcation path was not included in his analysis. A similar result to Huang has been obtained by Archer and Familli [2] and for low values of λ by Parmerter [10].

The comparison of the theoretical and experimental results has been carried out on the basis of the shallowness criterion obtained by Reissner [11] from an order of magnitude analysis of the equations governing the symmetrical deformation behaviour of the shallow shell. He concluded that all the test shells should conform to the criterion

$$\frac{H}{a} \lesssim \frac{1}{6}$$

if a valid comparison was to be made.

Some recent experiments on very accurate test shells have been made by Loo and Evan-Iwanowski [8], Parmerter [10] and Krenzke and Kiernan [7] and their results for the observed buckling loads are shown plotted in Fig. 3. All of these test shells came within the Reissner criterion. Deflection measurements were made across a diameter of the shells before buckling occurred by the workers in [8] and [10] and a variation in the symmetrically deformed shape of the shell with λ was observed. No attempt was made to measure asymmetrical displacements. All of the above experimental workers observed that the final buckled configuration of each shell was always a single edge dimple (i.e. $n = 1$).

In the present paper the stability of the first two asymmetrical modes after the Huang bifurcation point is investigated theoretically on the basis of Marguerre's [9] non-linear shallow shell equations. Two modes only are considered in an attempt to reduce the amount of computational work involved. An approximate solution is found by using the Ritz–Galerkin method. Results are also presented of a detailed experimental investigation of the asymmetrical buckling of model shallow clamped caps in which asymmetrical deformation modes are detected and measured for the first time. These results together with the present theoretical results casts doubt on the validity of Reissner's [11] shallowness limit being carried on over into the region of asymmetrical deformation; something which has been the practice of all previous experimental workers. The experiments are carried on into the region of symmetrical behaviour and the results obtained for the snapping loads of nominally perfect and imperfect shells are compared with existing theory.

THEORY

Following previous workers [5, 10, 2] the analysis is made via Marguerre's [9] non-linear shell equations. By using these equations the results will only be applicable to shells which are both thin and shallow. The "shallowness limit" assumed by workers for the

spherical cap is usually $H/a < \frac{1}{6}$ or, sometimes, $H/a < \frac{1}{8}$. It will be shown later that, where asymmetrical displacements are concerned, these values may be optimistic.

The following notation is used

$$\frac{\partial}{\partial r}(\ ) = (\ )' \qquad \frac{\partial}{\partial \theta}(\ ) = (\dot{}).$$

Higher and cross derivations are indicated by multiple indices. For equilibrium of the in-plane forces in the shell

$$(rN_r)' + \dot{N}_{r\theta} - N_\theta = 0 \tag{1}$$

$$(rN_{r\theta})' + \dot{N}_\theta + N_{r\theta} = 0 \tag{2}$$

where N_r, N_θ are in the in-plane forces per unit length in the meridional and circumferential directions respectively and $N_{r\theta}$ is the corresponding shear force. Equations (1) and (2) can be satisfied by a stress function F where

$$N_r = \frac{1}{r}F' + \frac{1}{r^2}\ddot{F} \tag{3}$$

$$N_\theta = F'' \tag{4}$$

$$N_{r\theta} = -\left(\frac{1}{r}\dot{F}\right)'. \tag{5}$$

The corresponding membrane strains are given by

$$\varepsilon_r = \frac{1}{tE}(N_r - \nu N_\theta) \tag{6}$$

$$\varepsilon_\theta = \frac{1}{tE}(N_\theta - \nu N_r) \tag{7}$$

$$\gamma_{r\theta} = \frac{2}{tE}(1+\nu)N_{r\theta}. \tag{8}$$

The non-linear displacement relations can be expressed by

$$\varepsilon_r = U' + \frac{r}{R}W' + \frac{1}{2}(W')^2 \tag{9}$$

$$\varepsilon_\theta = \frac{U}{r} + \frac{\dot{V}}{r} + \frac{1}{2}\left(\frac{1}{r}\dot{W}\right)^2 \tag{10}$$

$$\gamma_{r\theta} = \frac{\dot{U}}{r} - \frac{V}{r} + V' + \frac{1}{r}\dot{W}W' + \frac{r}{R}\dot{W}. \tag{11}$$

Introducing the quantity

$$x = \frac{r}{a} \tag{12}$$

and the notation

$$\frac{\partial}{\partial x}(\ ) = (\ )^*.$$

Marguerre's shallow shell equations can be written as

$$D\nabla^4 W+\frac{1}{a^4}\left[\frac{2}{x^2}\dot{F}^*\dot{W}^*+\frac{2}{x^4}\dot{F}\dot{W}-\frac{1}{x}F^*W^{**}-\frac{1}{x}F^{**}W^* -\frac{1}{x^2}F^{**}\ddot{W}-\frac{1}{x^2}\ddot{F}W^{**}-\frac{2}{x^3}\dot{F}^*\dot{W}-\frac{2}{x^3}\dot{F}\dot{W}^*\right]-\frac{2H}{a^4}\left[F^{**}+\frac{F^*}{x}+\frac{\ddot{F}}{x^2}\right]-P=0 \tag{13}$$

$$\frac{a^4}{Et}\nabla^4 F-\left[\frac{1}{x^2}(\dot{W}^*)^2+\frac{1}{x^4}(\dot{W})^2-\frac{1}{x}W^{**}W^*-\frac{1}{x^2}W^{**}\ddot{W} -\frac{2}{x^3}\dot{W}^*\dot{W}\right]+2H\left[W^{**}+\frac{W^*}{x}+\frac{\ddot{W}}{x^2}\right]=0 \tag{14}$$

where P is the applied pressure,

$$\nabla^4(\ )=\frac{1}{a^4}\left[(\ )^{****}+\frac{2}{x}(\ )^{***}-\frac{1}{x^2}(\ )^{**}+\frac{1}{x^3}(\ )^*+\frac{4}{x^4}(\ddot{})-\frac{2}{x^3}(\ddot{})^*+\frac{2}{x^2}(\ddot{})^{**}+\frac{1}{x^4}(\ddot{})^{**}\right] \tag{15}$$

and

$$D=\frac{Et^3}{12(1-\nu^2)}$$

Equation (13) is the out of plane equilibrium equation and (14) the compatibility equation for a deformed shell element.

Boundary conditions

Since the shell is clamped along a parallel circle

$$U=V=W=W'=0 \qquad \text{when} \quad r=a. \tag{16}$$

From these conditions it follows from the strain–displacement relations that

$$\left.\begin{aligned}\varepsilon_\theta &= 0\\ a\varepsilon_\theta'-\varepsilon_r-\dot{\gamma}_{r\theta} &= 0\end{aligned}\right\} \quad \text{when} \quad r=a. \tag{17}$$

and

Furthermore at the centre of the shell we must have

$$\left.\begin{aligned}&W \text{ finite}\\ &\text{All stresses finite}\end{aligned}\right\} \quad \text{when} \quad r=0. \tag{18}$$

The conditions (17) can be expressed in terms of the stress function F by means of (3)–(8) and (12) as

$$\left.\begin{aligned}3F^{**}-F^*-\ddot{F} &= 0\\ 3F^{***}-2F^*+7\dot{F}^*-9\ddot{F} &= 0\end{aligned}\right\} \quad \text{when} \quad x=1 \tag{19}$$

here and henceforth the value of ν has been taken as $\frac{1}{3}$.

Using equations (3)–(5) and (12) the conditions (18) can be expressed as

$$\left.\begin{aligned} &\frac{1}{xa^2}F^* + \frac{1}{x^2a^2}\dot{F} \\ &\frac{1}{a^2}F^{**} \\ &-\frac{1}{a}\left[\frac{1}{xa}\dot{F}\right]^* \end{aligned}\right\} \text{ finite when } \quad x = 0. \tag{20}$$

Reduction of the equations

Because of the complexity of Marguerre's equations it was decided to obtain an approximate solution of them by the Ritz–Galerkin method. The method consists of assuming the deflected shape of the shell as a linear combination of suitably chosen functions each satisfying the geometrical boundary conditions of the problem. Each function is multiplied by a deflection parameter which is then adjusted by Galerkin's method to optimize the solution over the region of interest.

Three functions are chosen to represent the change in the symmetrically deformed shape of the shell with λ (see for example experimental results in reference [10]) and are as follows

$$\left.\begin{aligned} W_1 &= (1-x^2)^2 \\ W_2 &= x^2(1-x^2)^2 \\ W_3 &= x^2(1-x^2)^2(1-4x^2). \end{aligned}\right\} \tag{21a, b, c}$$

With this number of symmetrical terms used the results should be valid for $\lambda \lesssim 8$. The $n = 1$ and $n = 2$ asymmetrical mode functions are chosen to represent closely the shapes deduced by Huang [5]. They are (for the $n = 1$ and $n = 2$ modes respectively):

$$\left.\begin{aligned} W_4 &= x(1-x^2)^2 \cos\theta \\ W_5 &= x^2(1-x^2)^2 \cos 2\theta \end{aligned}\right\} \tag{22a, b}$$

All of the above shapes satisfy the necessary geometrical boundary conditions of the problem. When each deflection function is multiplied by a free parameter the complete deflection function is formed from their sum as:

$$W = (1-x^2)^2(A + Bx^2 + Cx^2(1-4x^2) + Jx\cos\theta + Kx^2\cos 2\theta). \tag{23}$$

Determination of the stress function

The deflection function (23) is now substituted into (14) and an expression for F is obtained in the form

$$\nabla^4 F = f(x, \theta). \tag{24}$$

By expressing F as an infinite cosine series of the form

$$F = \sum_{s=0}^{\infty} F_s \cos s\theta$$

and substituting into (15) a further expression for $\nabla^4 F$ is obtained as

$$\nabla^4 F = \frac{1}{a^4}\sum_{s=0}^{\infty}\left[F_s^{****} + \frac{2}{x}F_s^{***} - \frac{(1-2s^2)}{x^2}F_s^{**} + \frac{(1+2s^2)}{x^3}F_s^{*} + \frac{s^2(s^2-4)}{x^4}F_s\right]\cos s\theta. \tag{25}$$

A comparison of the terms in (24) and (25) yields an infinite set of fourth order differential equations for determining the coefficients F_s. Each of these equations can be integrated without difficulty (the integrands being simple polynomials in x) and yield four constants which are chosen to satisfy the stress boundary conditions (19) and (20). It was found that for $s > 4$ the coefficient F_s must become identically zero if these conditions were to be satisfied and hence an exact solution to the compatibility equation was obtained.

Reduction to a set of non-linear algebraic equations

Substituting F into (13) and applying Galerkin's method (i.e. multiplying through by the deflection functions (21) and (22), in turn, and integrating over the range of definition of the variables) leads to five non-linear algebraic equations for determining the deflection parameters for any assumed value of the load. These equations can be non-dimensionalized by introducing

$$A_d = \frac{A}{H}, B_d = \frac{B}{H}, \text{etc.} \qquad \lambda^4 = \frac{128}{3}\left(\frac{H}{t}\right)^2$$

$$P_0 = \frac{32EH^3t}{\lambda^2 a^4} \qquad q = \frac{P}{P_0}.$$

These final equations are not written down here explicitly because of their length. However full details can be found in [13]. The equations governing either symmetrical, asymmetrical bifurcation or asymmetrical post-bifurcation behaviour can be obtained from them simply by equating the unwanted deflection parameters to zero. In the bifurcation problem for example the equations reduce to three which describe the symmetrical behaviour of the cap together with two side conditions which must be satisfied if an asymmetrical bifurcation point is to exist on the symmetrical loading path. For the post-bifurcation behaviour case four equations must be solved together with a side condition which must be satisfied if a transition path bifurcation point is to exist. (Details of these transition points are given in the next section.)

Each set of equations were solved numerically on a computer, using the generalized Newton–Raphson iterative algorithm described by Householder [4], without difficulty.

Theoretical results

The results obtained for the snapping and bifurcation pressures for varying λ are shown in Fig. 4. A comparison has been made here with the theories of Huang [5] and Budiansky [3].

The results for the post-bifurcation paths of the $n = 1$ and $n = 2$ asymmetrical modes for $\lambda = 6$ are shown in Fig. 5. Both paths have been followed some way into the asymmetrical region and in the case $n = 2$ the path has been followed until it rejoins the

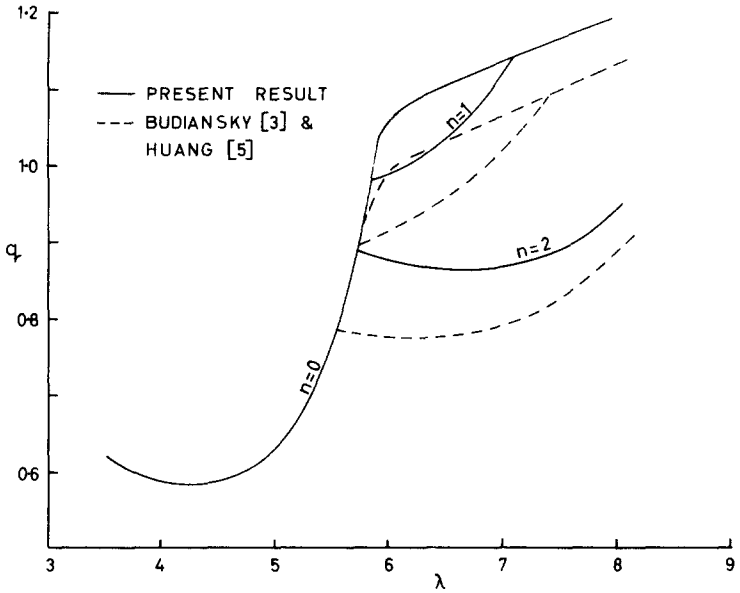

FIG. 4. Present theoretical snapping and bifurcation pressures.

symmetrical deformation curve (not shown in the figure). The quantity V_d in this Figure is defined later.

A search was made for a transition path joining the $n = 2$ to the $n = 1$ post-bifurcation paths in an attempt to explain why the test shell always favours the $n = 1$ pattern at failure. The line of argument followed was that somewhere along an $n = 2$ post-bifurcation path it might be possible for another bifurcation to occur which would be into a mode made up of

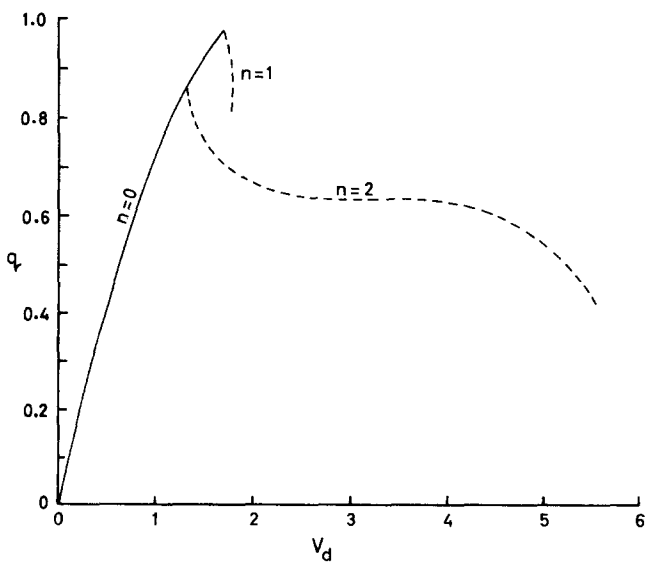

FIG. 5. Theoretical equilibrium paths for modes $n = 1$ and $n = 2$ when $\lambda = 6$.

a combination of the $n = 1$ and $n = 2$ deformation modes. This transition path would then join the $n = 1$ post-bifurcation path allowing the shell to assume its final buckled shape. However, no such transition path bifurcation points were found.

EXPERIMENTAL METHOD

Shell specimens

Any elastic buckling test on shallow caps involves large deformations of the test specimens and, in consequence, the possibility of yielding of the shell material. In view of this the test shells were manufactured by vacuum pressing hot rigid-polyvinylchloride (PVC) plastic sheet against accurately turned spherical metal moulds of the required radius. The PVC sheet chosen had been specially developed by Imperial Chemical Industries (I.C.I.) for vacuum forming and was capable of being considerably stretched when hot without undue thinning. All the physical and chemical properties of this material have been thoroughly investigated by I.C.I. and are listed in their handbook [6]. Independent checks on the values for the elastic modulus, Poisson's ratio and creep rate were carried out in the laboratory. These checks confirmed the handbook values and the small creep rate of the material at room temperature. The linearity of the PVC was good up to stresses of 3500 lb/in^2. The metal moulds were turned from duralumin in the lathe by means of a specially designed spring loaded tool which fitted in the cross slide and followed an accurate template of the required radius fitted in the tailstock. Details of this device can be obtained from Reference [13]. The shell manufacturing procedure was to clamp a piece of the PVC sheet over the mould and heat the latter to 100°C in an electric oven for about 30 min during which time the sheet became soft. The air was then removed from between the mould and the sheet by means of a vacuum pump, which forced the sheet to conform to the mould's contours. With the vacuum maintained the mould was allowed to cool to room temperature. Subsequent tests showed that the shells produced were of good profile (maximum measured deviation was $+2\%$ over the mould radius) and thickness variation (no variations above $\pm 2\%$ of the mean thickness were found) and, because the load capable of being carried by the hot sheet was virtually zero, the initial stresses induced in the material were negligible.

Loading apparatus

The rigid loading device used to test the present shells is shown schematically in Fig. 6. The shell forms a membrane separating the two volumes of water A and B. The volume of water A can be put under a pressure, suitable to buckle the shell, by means of the pump which transfers water from the reservoir into the vessel. This initial pressurization is carried out with the equalizing valve open so that A and B are connected and no load is applied to the shell. If A and B are now isolated the shell can be displaced through a known volume by opening the volume displacement valve. When this valve is closed a pressure differential is set up between A and B which is equivalent to the load carried by the shell. In order to maintain rigidity this pressure differential was measured by means of an initially calibrated differential pressure transducer which gave a linear output over its working range of ± 5 lb/in^2. The total movement of the measuring element over this range was only 0·0015 in.

Deformation measurements

The deflections of prime interest were the asymmetrical deformations occurring, according to Huang's theory, in the circumferential directions in shells of $\lambda > 5{\cdot}5$. The device

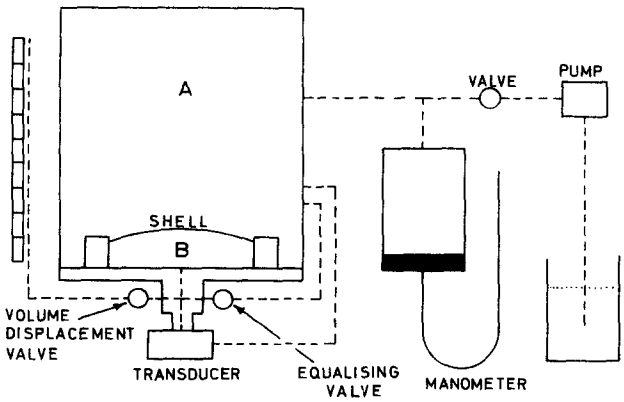

FIG. 6. Schematic diagram of the loading device.

shown in Fig. 7 was developed for this purpose. It consisted essentially of an eccentrically placed small ($\frac{1}{4}$ in. diameter) silver metal probe which continuously rotated over the surface of the shell a small distance from it. Subsequent measurement of the resistance of the water gap between the probe tip and the shell surface enabled both symmetrical and asymmetrical displacements to be determined for the particular eccentric radius chosen. Each PVC shell was coated with a molecular thin layer of silver metal by the well known "silver mirror process" to enable it to conduct the current. (The process consists of chemically reducing silver nitrate to silver metal and is carried out at 15°C thus ensuring the shells are not warped by any heating effects). Since both the inside and outside surface of each shell were covered in this process the radius of each shell would be checked optically by using it as a concave mirror. The water gap between the shell and probe tip was included as one arm in an A.C. resistance bridge, the modulated output of which was fed through an amplifier and demodulator to a U.V. pen recorder which gave a continuous record on paper strip. The output from the pressure transducer was fed via a D.C. amplifier to another pen on the recorder. The probe was rotated continuously during each test by a small motor and each complete revolution was also recorded on the final output. Each 0·1 cc of volume displacement of each shell was also recorded on the trace by means of a manually operated switch.

Testing method

Each silvered shell was fitted into the loading device by clamping it between correctly contoured rings. The clamping was done systematically to ensure an even pressure around the shell boundary. With the drive shaft of the probe central over the shell the resistance gap was set to about $\frac{1}{25}$ in. and an initial profile scan, at zero load, was made. The shell was then loaded continuously but very slowly until buckling occurred (the average time for this to occur being about 4 min). The load was then removed and calibration tests were carried out to relate the load and displacement traces recorded to actual physical quantities.

EXPERIMENTAL RESULTS

(i) *Results from complete shells with* $\lambda < 5{\cdot}5$

A total of eighteen shells of low λ value were tested in the present work and three different values of the parameter H/a were employed. All the shells came within the shallowness limit. All the tests were carried out without using the deflection probe and the load was

measured directly by means of a micropotentiometer. The observed post-snapping path for shells in the range $3{\cdot}8 \leq \lambda \leq 4{\cdot}6$ became more peaked as λ increased and for shells of $\lambda > 4{\cdot}6$ the path became "backwards" (Fig. 2) and could not be followed in the present rig. For these shells a jump at constant volume into a rotationally symmetrical dimple occurred when the critical load was reached. It is unknown if this jump was made via any asymmetrical deformation. The geometry of each shell and the corresponding observed snapping loads are shown in Table 1. A comparison of the observed snapping loads and the theory of Budiansky is shown in Fig. 8.

TABLE 1

Shell no.	R in.	$t \times 10^3$ in.	H/a	λ	Snapping load lb/in^2
B47/1	18·98	46·7	0·052	3·86	2·16
B47/2	18·98	46·0	0·052	3·89	2·09
B47/3	18·98	46·6	0·052	3·86	2·07
B30/1	18·98	32·2	0·052	4·65	0·91
B30/2	18·98	32·4	0·052	4·64	0·90
B30/3	18·98	30·9	0·052	4·75	0·94
B30/4	18·98	31·2	0·052	4·72	0·91
B30/5	18·98	30·6	0·052	4·77	0·87
B30/6	18·98	28·9	0·052	4·91	0·87
B30/7	18·98	27·0	0·052	4·92	0·86
B30/8	18·98	27·9	0·052	5·00	0·86
B25/1	18·99	24·9	0·052	5·29	0·63
B25/2	18·99	24·4	0·052	5·34	0·61
B25/3	18·99	23·9	0·052	5·39	0·59
C30/1	24·99	29·3	0·040	4·25	0·43
C30/2	24·99	28·1	0·040	4·34	0·41
C20/1	24·99	19·9	0·040	5·15	0·23
D30/1	13·99	31·2	0·074	5·15	1·80

In all cases the base radius a was 2·000 in. All test data was reduced by using $E = 450{,}000$ lb/in^2 and $\nu = 0{\cdot}3$ at 20°C for the P.V.C. sheet.

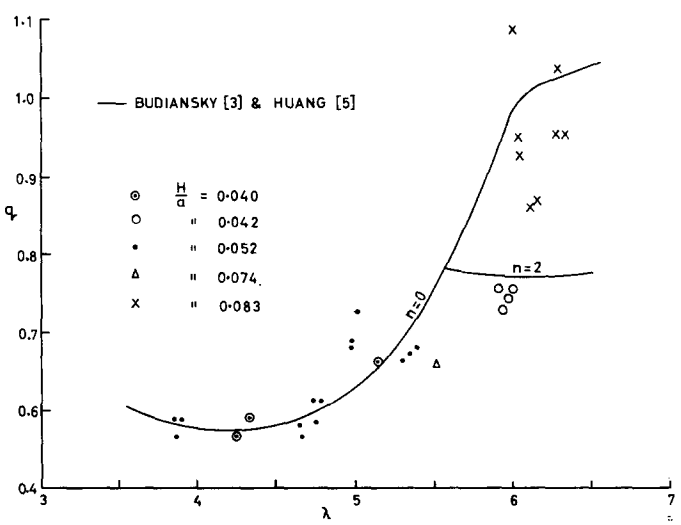

FIG. 8. Present experimental results.

(ii) *Results from imperfect shells*

Tests were carried out on imperfect shells of $\lambda = 5{\cdot}0$. All the shells were nominally of the same radius of curvature, mean thickness and base radius. The imperfections consisted of axisymmetrical circular flats of varying diameter and the results obtained for the loading paths for these shells are shown in Fig. 9. The dimensions of the specimens are included in this figure. The quantity V_d is the dimensionless volume displacement and is given by

$$V_d = \frac{\lambda^2}{2H} \frac{V_R}{\pi a^2}$$

where V_R is the actual displaced volume of the shell.

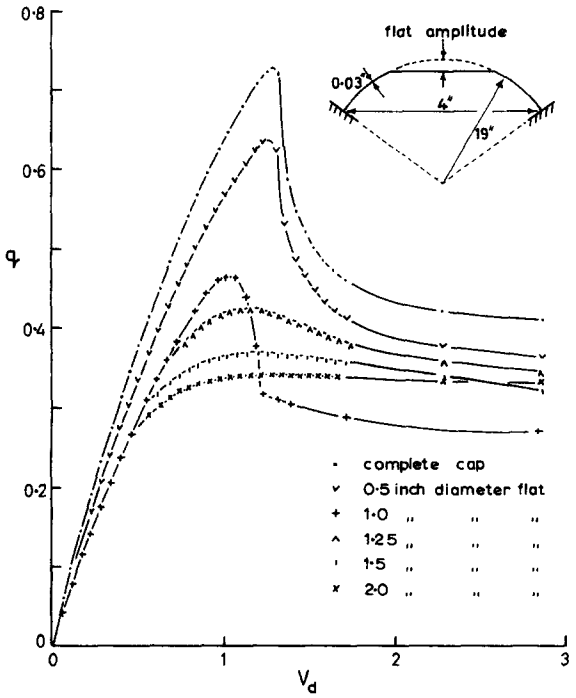

FIG. 9. Experimental symmetrical equilibrium paths from imperfect shells.

Each loading line corresponds to at least two different tests obtained from nominally identical shells. It was found that there was very close agreement between these loading paths and this included the unexpected result from the 1 in. diameter flat. In Fig. 10 the critical loads are compared with the theory given by Budiansky [3].

(iii) *Results from shells of* $\lambda \cong 6$

A total of 12 shells of $\lambda \cong 6$ were tested and two values of H/a were employed. The geometry, etc., of these shells are shown in Table 2. The final observed buckling loads are plotted in Fig. 8. One is struck immediately by the high buckling loads and large scatter from the shells of $H/a = 0{\cdot}083$. The deflection probe was used during these tests and the probe tip was set at a distance of 1·1 in. from the shell's centre in all cases. This distance

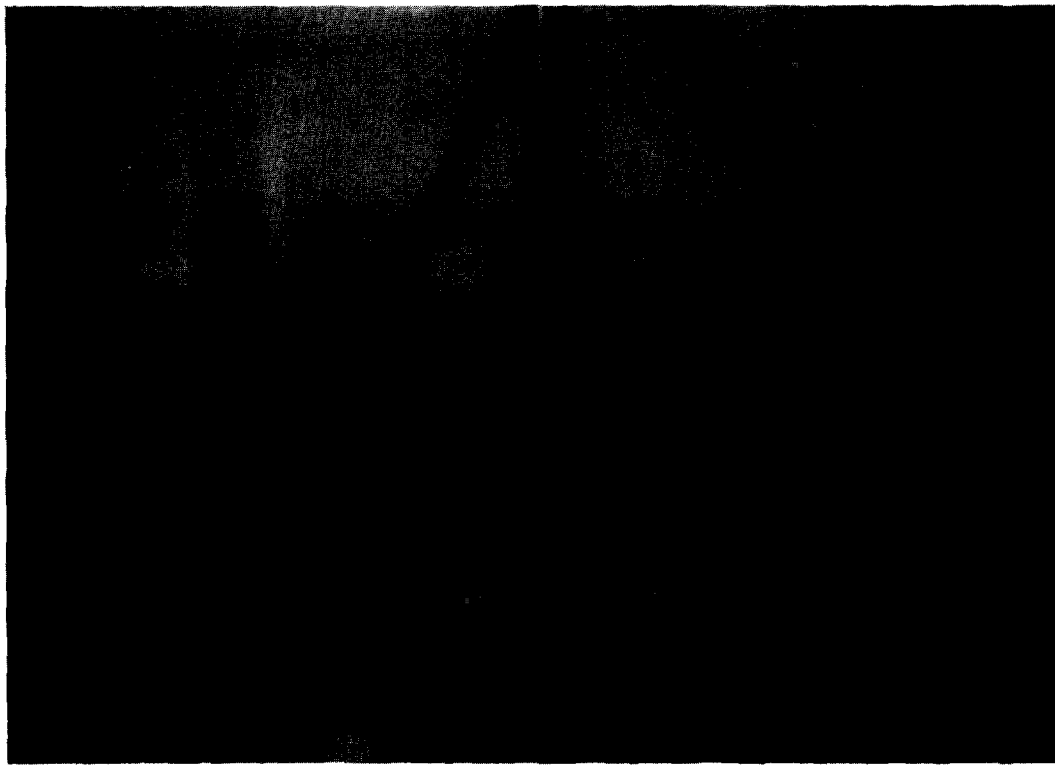

FIG. 7. Asymmetrical deflection measuring probe.

[*facing page* 48

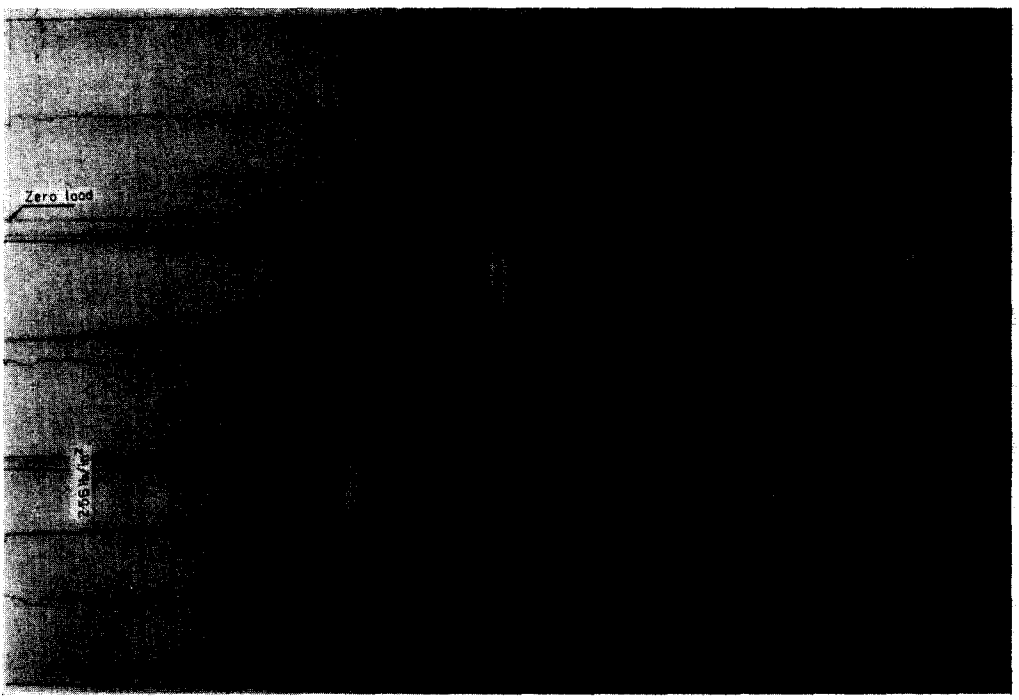

FIG. 11. Typical output trace obtained from shells of high H/a ratio.

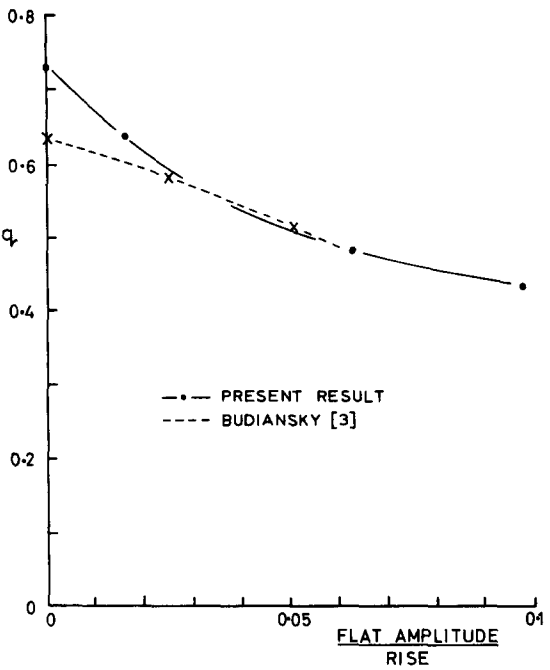

FIG. 10. Experimental snapping loads from imperfect shells compared with theory.

was chosen to correspond to Huang's prediction as to the point where maximum mode $n = 2$ deformation should occur. The paper strip output obtained for each shell contained a record of any asymmetrical deformations that occurred together with the load carried. It was found for the shells of $H/a = 0{\cdot}083$ that stable $n = 2$ asymmetrical modes always occurred before the usual unstable jump into the single edge dimple type of failure. Three parts of a typical load-deformation output trace from one of these shells are shown in Fig. 11. In this figure the line rising from the bottom of the trace represents the increasing load being carried by the shell and the line running approximately down the centre the

TABLE 2

Shell no.	R in.	$t \times 10^3$ in.	H/a	λ	Final buckling load lb/in^2
TS1	11·98	29·2	0·083	6·14	2·80
TS2	11·98	27·8	0·083	6·29	3·13
TS3	11·98	30·8	0·083	5·99	3·92
TS4	11·98	29·2	0·083	6·14	2·82
TS5	11·98	29·9	0·083	6·06	3·18
TS6	11·98	28·0	0·083	6·27	2·86
TS7	11·98	30·4	0·083	6·02	3·36
TS8	11·98	27·7	0·083	6·32	2·77
TS9	23·99	15·8	0·042	5·91	0·18
TS10	23·99	15·5	0·042	5·96	0·17
TS11	23·99	15·6	0·042	5·93	0·17
TS12	23·99	15·4	0·042	5·98	0·17

In all cases the base radius a was 2·000 in.

circumferential profile. If the deformations are axisymmetric this line will remain essentially straight but will move downwards. However, if asymmetrical deformations occur this line will wave in sympathy with them over each revolution of the probe. The small equally spaced marks at the top of the trace represent a complete revolution of the probe. As can be seen as the load increases axisymmetrical deformation occur first but asymmetrical displacements soon follow. Towards the end of the trace it is easy to distinguish a mode $n = 2$ displacement pattern; that is there are two alternate peaks and dimples per revolution around the shell. It is clear however, that even with this mode fully developed the shell is still carrying load as is evidenced by the still rising load line. The final buckling load is obtained when the shell jumps into the $n = 1$ mode with an immediate drop in the load carried. The maximum amplitude of all the $n = 2$ modes observed before the final $n = 1$ jump occurred was only 0·18 of the thickness. The results from this type of test on the shells of $H/a = 0{\cdot}042$ were negative in the sense that no asymmetrical deformations were detected before the final jump into the $n = 1$ mode occurred. By Fourier analysing some of the traces it was possible to obtain load-asymmetrical mode amplitude plots for several nominally identical shells, and the results from this are shown in Fig. 12. Here the last plotted experimental point on each curve represents the moment of jumping to the $n = 1$ mode.

DISCUSSION

The snapping loads observed for shells of $\lambda < 5{\cdot}5$ (Fig. 8) show excellent agreement with the theory of Budiansky [3] and the effect of the parameter H/a on the snapping loads seems to be small. This last result is in agreement with the work of Reissner [11]. The high

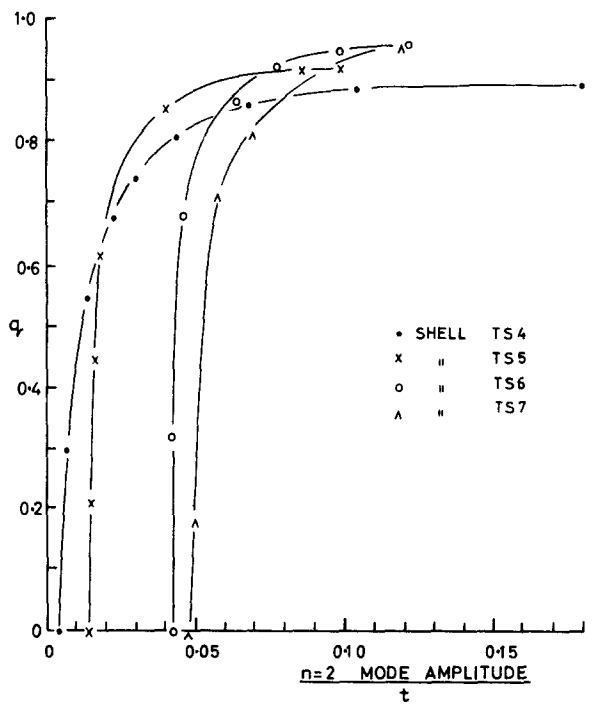

FIG. 12. The effect of initial $n = 2$ imperfection on shells of high H/a ratio.

results obtained by Loo and Evan-Iwanowski (Fig. 3) in this region are not repeated in the present work. The results shown in Fig. 10 for the effect of known imperfections on the snapping loads of nominally identical shells show a similar trend to that found theoretically by Budiansky [3]. The comparison is not strictly valid however as Budiansky used a slightly different axisymmetric imperfection shape. An interesting observation is that the imperfect shells all tend to approximately the same post snapping load as the deformations become large (Fig. 9).

The theoretical results obtained for the snapping pressures and bifurcation pressures of the $n = 1$ and $n = 2$ asymmetrical modes with varying λ (Fig. 4) show agreement with the work of Budiansky [3] and Huang [5]. The discrepancy between their results and the present one for $\lambda > 6$ is probably due to the limited number of assumed forms taken to represent the symmetrical and asymmetrical deformed shape of the shell in this region. The results obtained for the post-bifurcation behaviour of the $n = 1$ and $n = 2$ asymmetrical modes (Fig. 5) indicate they are both highly unstable; each equilibrium path exhibiting a small forwards slope at the bifurcation point. This implies any practical shell will be extremely sensitive to any initial imperfection in these modes. The result for the $n = 2$ mode is at variance with the present experimental results from shells of $\lambda \cong 6$ and $H/a = 0{\cdot}083$. All these shells exhibited a stable $n = 2$ mode (Fig. 11) and indeed initial imperfections in this mode seemed to increase the load at which final instability occurred (Fig. 12). It is possible that the higher order modes (i.e. $n = 3, 4$, etc.) are also stable in shells of "large" H/a ratio and the buckling loads obtained by Parmerter and Evan-Iwanowski/Loo (Fig. 3) for shells with $H/a \geq 0{\cdot}1$ support this idea. The shallower shells of $H/a = 0{\cdot}042$ all fell below the $n = 2$ bifurcation curve and seem to have behaved as the theory has predicted. However no $n = 2$ modes was detected, even with the present "rigid" apparatus, which suggests that for these shells the $n = 2$ path exhibits a "backwards" slope at the bifurcation point.

The fruitless theoretical search for a transition path joining the $n = 2$ to the $n = 1$ post-bifurcation path may mean that no such transitions are valid. If this is true the final $n = 1$ mode observed in test shells by previous workers (and in the present case) must be triggered by imperfections. It is clear from the present experiments that the $n = 1$ mode is highly unstable, ("backwards" slope) and in consequence imperfections in this mode will have a drastic effect on the final buckling load. However, it may be that higher order modes, not considered here, may play some part in any possible coupling between the two modes examined in the present work and hence the present negative theoretical result cannot be taken as being conclusive.

CONCLUSIONS

It is clear from the experimental work on shells of $\lambda < 5{\cdot}5$ that excellent agreement can be obtained with the existing theory of Budiansky [3] provided care is taken in manufacturing and testing the shell specimens. Also, if the shells lie within the Reissner [11] shallowness limit the effect of the parameter H/a on the snapping loads of shells of similar λ is small. Tests on shells of $\lambda = 5$ and having known size of initial imperfection show the expected large decrease in overall load carrying capacity when quite small imperfections are present and the change in snapping load with imperfection size shows a similar trend to that found theoretically by Budiansky [3].

The theoretical results obtained for the behaviour of the $n = 1$ and $n = 2$ asymmetrical modes show they are both unstable after the bifurcation point. This result is at variance

with the present experimental results obtained from shells of $\lambda \cong 6$ and $H/a = 0{\cdot}083$ which exhibited a stable $n = 2$ asymmetrical mode before finally buckling in the usual single edge dimple configuration. Shells in this region having $H/a = 0{\cdot}042$ seem to have behaved as the theory has predicted. The difference in these two results would suggest that the parameter H/a greatly effects the stability of shells in this region and that the shallowness limit must be set at much less than 1/6 (or 1/8) if correlation is to be obtained with shallow shell theory. It is possible that the stability of the higher order asymmetrical modes may also exhibit a dependence on the H/a parameter. The experimental results in [10] and [8] support to this idea.

An analysis of the post-bifurcation behaviour of a non-shallow cap, in which the geometry depends on both λ and H/a, is needed to finally clear up this point.

A theoretical investigation of the branching behaviour of the various asymmetrical modes has been undertaken by J. R. Fitch at Harvard University and he has arrived at the same qualitative results found here. (i.e. unstable $n = 1$ and $n = 2$ behaviour). From his analysis, which was essentially more accurate than the one presented here, he also found a "backwards" slope to the $n = 2$ bifurcation path (Private communication—May 1967).

REFERENCES

[1] R. R. ARCHER, *Q. appl. Math.* **15**, 355 (1958).
[2] R. R. ARCHER and J. FAMILLI, *J. appl. Mech.* **31**, 116 (1965).
[3] B. BUDIANSKY, *Proc. Symp. on the Theory of Thin Elastic Shells.* p. 64. North Holland (1950).
[4] A. S. HOUSEHOLDER, *Principles of Numerical Analysis*, p. 86. McGraw-Hill (1953).
[5] N. C. HUANG, *J. appl. Mech.* **30**, 447 (1964).
[6] I.C.I. *Handbook of Darvic and Flovic P.V.C. Sheet*, Imperial Chemical Industries.
[7] M. A. KRENZKE and T. J. KIERNAN, *AIAA Jnl.* **1**, 2855 (1963).
[8] R. M. EVAN-IWANOWSKI and T. C. LOO, Tech. Rep. 834 (II) No. 4 Syracuse University Research Institute.
[9] K. MARGUERRE, *Jb. dt. LuftForsch*, 413 (1939).
[10] R. R. PARMERTER, AFOSR 5362 Rep. Calif. Inst. of Tech. (1963).
[11] E. REISSNER, *J. Math. Mech.* **7**, 121 (1958).
[12] G. A. THURSTON, *J. appl. Mech.* **28**, 557 (1961).
[13] S. C. TILLMAN, Ph.D. Thesis, University of London (1965).
[14] H. J. WEINITSCHKE, *J. Math. Phys.* **38**, 209 (1959).

(*Received* 27 *January* 1969; *revised* 19 *May* 1969)

Абстракт—Даются результаты теоретических и экспериментальных исследований упругой устойчивости защемленных пологих сферических крышек, подверженных одномерному давлению. Обращается внимание на геометрический параметр λ, для которого справедливы симметрические и две первые антисиимметрические формы деформации. Для симметрического случая результаты идеально согласовываются с существительной теорией номинально идеальных оболочек и оболочек с известной величиной неправильности. Для антисимметрического случая теоретическая работа определяет неустойчивость двух форм деформации выше точки бифуркации, а также отсутствие переходной линии между ними. Тем не менее, экспериментальные результаты дают критическую зависимость между остаточной нагрузкой при потере устойчивости оболочек такого же самого параметра λ и рост к основному отношении радиуса. Оказывается, что начальные антисимметрические неправильности являются важными.